

# Temporal dissipative structures in optical Kerr resonators with transient loss fluctuation

YUANYUAN CHEN,<sup>1</sup> TUO LIU,<sup>1</sup> SUWAN SUN,<sup>1</sup> AND HAIRUN GUO<sup>1,\*</sup>

<sup>1</sup>Key Laboratory of Specialty Fiber Optics and Optical Access Networks,  
Joint International Research Laboratory of Specialty Fiber Optics and Advanced Communication,  
Shanghai Institute for Advanced Communication and Data Science,  
Shanghai University, Shanghai 200444, China  
\*hairun.guo@shu.edu.cn

**Abstract:** Dissipative structures are the result of spontaneous symmetry breaking in a dynamic open system, which is induced by either the nonlinear effect or loss fluctuations. While optical temporal dissipative solitons in nonlinear Kerr cavities has been widely studied, they are operated in a red-detuned regime that is non-trivial to access. Here, we demonstrate an emergent dissipative soliton state in optical cavities in the presence of loss fluctuations, which is accessible by self-evolution of the system and is operated in resonance. We numerically investigate both the effect of loss modulation and the effect of saturable absorption, based on a standard dissipative and Kerr-nonlinear microresonator model, and observe stable soliton states in a close-to-zero detuning region. The self-starting soliton state working in resonance is potentially of wide interest, which would not only ease the operation for ultrafast temporal soliton generation, but also imply a high conversion efficiency for soliton micro-combs.

© 2022 Optical Society of America under the terms of the [OSA Open Access Publishing Agreement](#)

## 1. Introduction

Dissipative structures are known as a reproducible steady state of a dynamical open system featuring energy or matter exchange in an environment, which have been widely observed and studied in thermodynamics, chemistry and biology [1], as well as in optics [2]. In particular, their observations in dissipative and nonlinear optical cavities have clarified the nature of mode locking among a set of Kerr induced intracavity laser components [3], in the form of a localized temporal soliton pattern [4, 5] and in spectrum corresponding to an equidistant frequency comb structure. Indeed, temporal dissipative solitons in optical microresonators have constituted a way to fully coherent optical frequency combs, with high-compactness and large repetition frequencies in the microwave range [6], and open the field of optical micro-comb in integrated nonlinear photonics as well as in chip-scale precise time and frequency measurement. This has unveiled a wide range of applications such as parallel coherent communications [7–10], optical ranging [11–13] and parallel LIDAR [14], low-noise microwave synthesis [15–17], astronomical spectrograph calibration [18, 19] and photonic neuromorphic computation [20, 21]. Fundamentally, the solitons are in a double-balance regime in both the energy and the momentum level. While the cavity dissipation is balanced by the optical parametric gain induced by an external pumping source, the dispersive effect is balanced by the nonlinearity. Yet, access to the soliton state is by artifice, as essential energy buildup is required to excite the nonlinear effect as well as the symmetry breaking of the system, which implies operations such as the laser frequency tuning [5, 22], modulated laser side-band tuning [23], or equivalently tuning the cavity resonance by thermal or piezoelectric effects [24, 25].

Several approaches have been reported to ease the operation. One effective way is to apply a fixed modulation on the pump wave that allows for self-evolution of the system to reach the soliton state, free from the laser tuning [26]. Other approaches include using an auxiliary laser to counterbalance the intracavity thermal effect and trigger the soliton burst [27], or employing laser

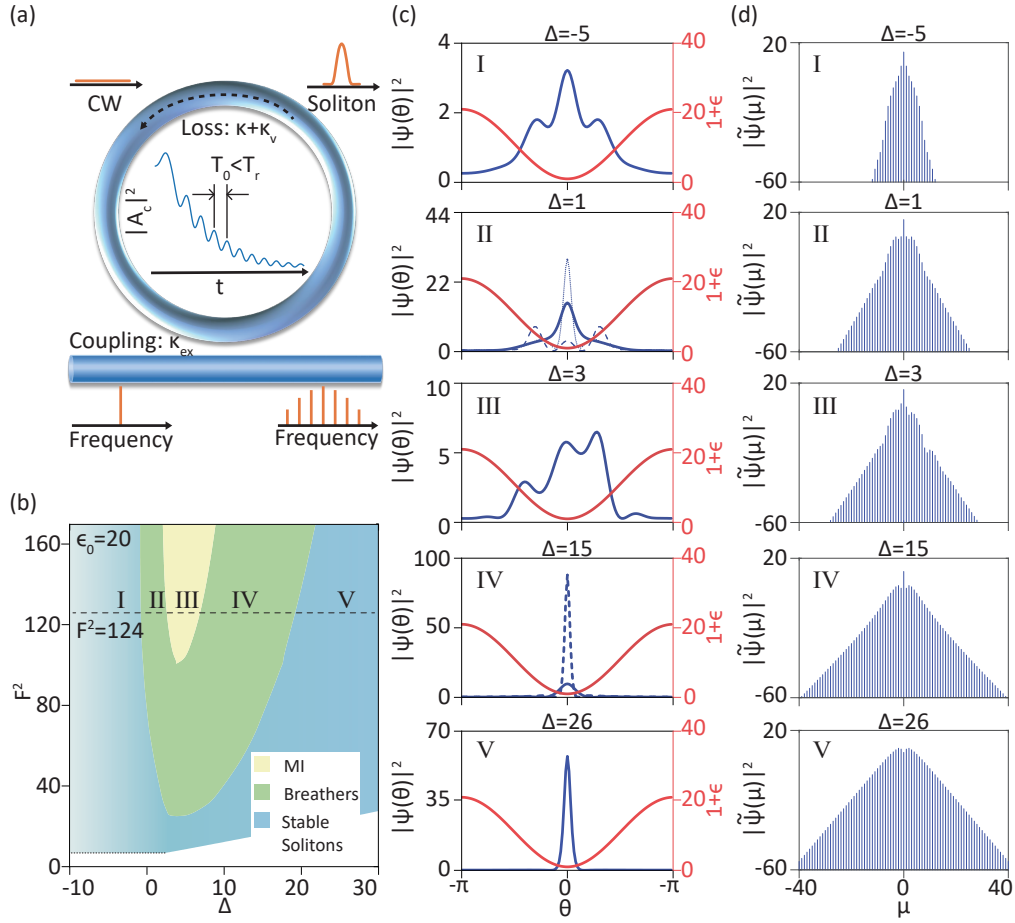


Fig. 1. Dissipative structures in microresonators via loss fluctuation. (a) A conceptual diagram of an optical microresonator in the presence of transient loss fluctuation. (b) Simulated stability chart of intracavity field patterns as a function of both the laser detuning  $\Delta$  and the pumping intensity  $F^2$ , in the condition that  $\epsilon_0 = 20$ , which consists of three types intracavity states, i.e. the MI state, the breathers, and the stable solitons. (c, d) Intracavity temporal profiles and the corresponding spectra of five consecutive states at  $F^2 = 124$ .

self-injection locking to the microresonator [15,28–30] which induces spontaneous pulling of the laser frequency, and enables turn-key operation for the soliton micro-comb generation [31,32] in a monolithic photonic chip with hybrid laser and microresonator integration [33,34]. Moreover, efforts have been made to combine dissipative systems with active materials, such as a graphene embedded microresonator that by altering the Fermi level enables gate-tunable cavity dispersion and charge-controlled soliton states [35]. In addition, active low-dimensional materials would also introduce switching on the cavity dissipation in the regime of saturable absorption (SA), which has been widely applied in mode locked lasers, resulting in dissipative soliton formation by self-evolution of the system. [36–38].

Nevertheless, in a standard optical dissipative and nonlinear cavity, it is suggested that temporal dissipative solitons are to be on the red detuned side of the resonance where the bifurcation of Kerr nonlinear induced symmetry breaking is present, and the soliton state at a close-to-zero

detuning region or in resonance is NOT supported.

Here, we investigate the soliton regime in dissipative optical cavities in the presence of transient loss fluctuations, and demonstrate that dissipative solitons are accessible by natural-evolution of the system working in resonance. We present a revised Lugiato-Lefever model [39] that includes the effect of loss modulation, as well as the effect of saturable absorption, and by simulations characterize the stable soliton state along with breathers, Turing rolls, and other localized temporal field patterns. Our work may contribute to enrich the dynamics of temporal dissipative solitons particularly in microresonator systems, and may represent a crucial step to establish a connected understanding between dissipative nonlinear systems and mode-locked laser systems, where spontaneous symmetry breaking is both induced by fluctuations on the cavity dissipation.

## 2. Numerical model

The concept of our work is illustrated in Fig. 1. In the presence of a periodic loss modulation, the photon energy in a dissipative cavity would experience an oscillatory decay over time, and in the condition that the oscillation period  $T_0 \leq T_r$  (where  $T_r$  is the cavity round-trip time), the effect of the loss fluctuation is transient. We limit ourselves to consider only Kerr nonlinearity in the cavity, second-order dispersive effect, and a continuous-wave (cw) driving source. Such a dissipative system can be described by the Lugiato-Lefever equation (LLE) [39], with an additional term  $\kappa_v(t, \vartheta)$  included corresponding to the effect of the loss fluctuation, which is:

$$\frac{\partial A(t, \vartheta)}{\partial t} = \left( -\frac{\kappa_v(t, \vartheta)}{2} - \frac{\kappa}{2} - i\delta_\omega - i\frac{D_2}{2} \frac{\partial^2}{\partial \vartheta^2} + ig|A(t, \vartheta)|^2 \right) A(t, \vartheta) + \sqrt{\frac{\kappa_{ex} P_{in}}{2\pi\hbar\omega_0}} \quad (1)$$

where  $A(t, \vartheta)$  is the temporal amplitude of the intracavity field, and the actuator  $\int_{-\pi}^{\pi} |A(t, \vartheta)|^2 d\vartheta$  indicates the overall number of intracavity photons. The constant loss rate  $\kappa$  consists of both the intrinsic loss rate  $\kappa_0$  in the cavity and the coupling loss rate  $\kappa_{ex}$ , i.e.  $\kappa = \kappa_0 + \kappa_{ex}$ . The laser cavity detuning,  $\delta_\omega$ , is defined as  $\delta_\omega = \omega_0 - \omega_p$ , where  $\omega_0$  is the angular frequency of the pumped central resonance and  $\omega_p$  is that of the cw pump.  $D_2$  indicates the second order dispersion in the cavity. The nonlinear coefficient,  $\gamma$ , indicates the efficiency of the nonlinear induced resonant frequency shift, with respect to the single photon energy ( $\hbar\omega_0$ ).  $P_{in}$  is the power of the cw pump.

The equation is further normalized to a dimensionless two-parameter model (i.e. in the panel of the laser detuning and the pump intensity), plus a perturbation on the loss, which is:

$$\frac{\partial \Psi(\tau, \varphi)}{\partial \tau} = \left( -\epsilon(\tau, \varphi) - 1 - i\Delta - i\frac{\partial^2}{\partial \varphi^2} + i|\Psi(\tau, \varphi)|^2 \right) \Psi(\tau, \varphi) + F \quad (2)$$

based on the following transformations:

$$\tau = \frac{\kappa}{2}t, \quad \varphi = \sqrt{\frac{\kappa}{D_2}}\vartheta, \quad \epsilon = \frac{\kappa_v}{\kappa}, \quad \Delta = \frac{2\delta_\omega}{\kappa}, \quad |\Psi(\tau, \varphi)|^2 = \frac{2g}{\kappa}|A(t, \vartheta)|^2, \quad F = \sqrt{\frac{8g\kappa_{ex}P_{in}}{2\pi\hbar\omega_0\kappa^3}} \quad (3)$$

In cases of periodically modulated loss factor, we have:

$$\epsilon(\tau, \varphi) = \epsilon_0 \left( 1 + \cos \left( N \sqrt{\frac{D_2}{\kappa}} \varphi + \pi \right) \right) \quad (4)$$

where  $\epsilon_0$  indicates the modulation depth of the transient loss,  $N$  is the number of modulation periods per round trip. It's worth noting that such a modulated loss factor is artificially introduced

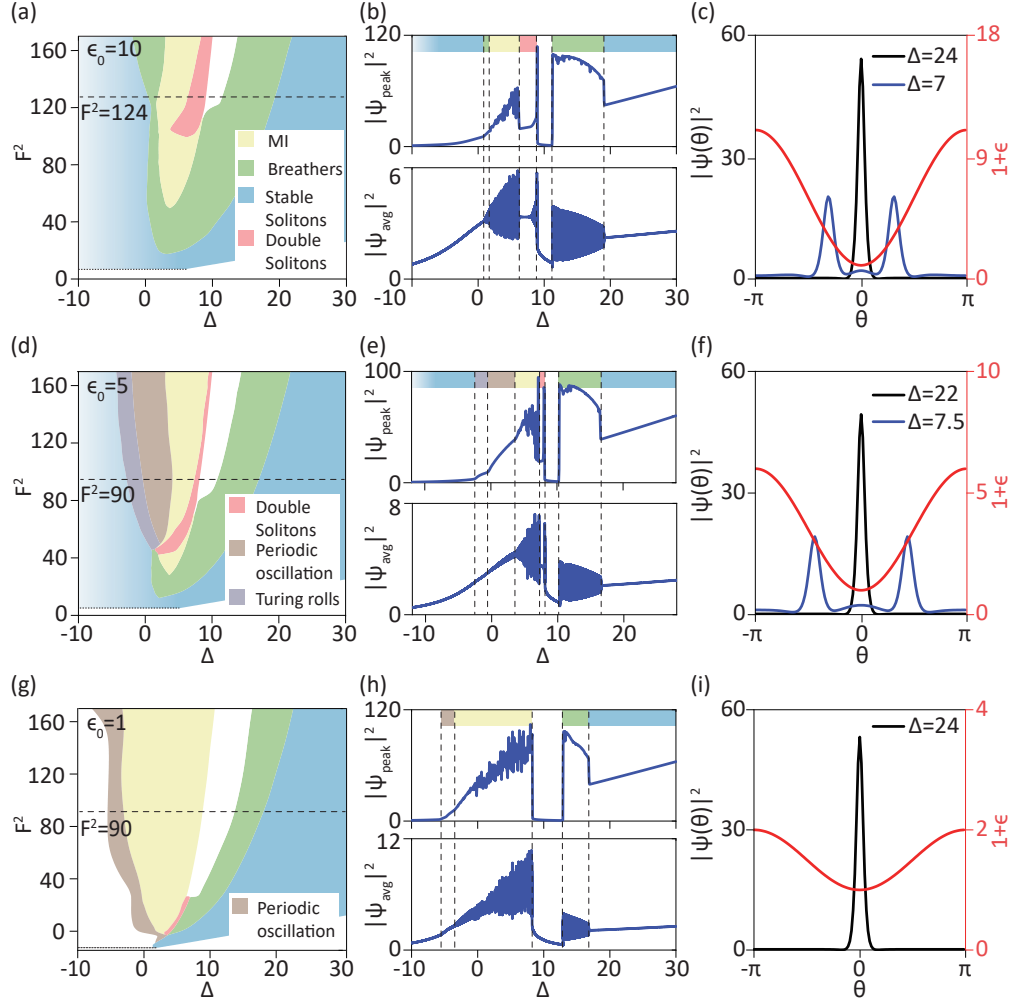


Fig. 2. Stability charts of dissipative structures. (a, d, g) Simulated stability charts of intracavity field patterns at three distinct modulation depths of the transient loss fact, i.e.  $\epsilon_0 = 10, 5$ , and  $1$ . (b, e, h) Selected traces of both the intracavity peak intensity and averaged intensity, as a function of the detuning, where clear boundaries for distinct dissipative structures can be recognized. (c, f, i) Intracavity field patterns on the red-detuned side and on the emergent stability region by loss modulations.

to the conventional LLE model and is independent on the intracavity field pattern. In contrast, a self-initiated loss fluctuation can be introduced to dissipative cavities in the regime of saturable absorption (SA), which is related to the intracavity field pattern [40], i.e.:

$$\frac{d}{d\varphi} \epsilon(\tau, \varphi) = -\frac{\epsilon(\tau, \varphi) - \epsilon_0}{\varphi_{SA}} - \epsilon(\tau, \varphi) \frac{|\Psi(\tau, \varphi)|^2}{E_{\varphi, SA}} \quad (5)$$

where  $\varphi_{SA}$  represents the recovery time of the saturable absorber, and  $E_{\varphi, SA}$  is the saturable energy. In the regime of fast SA (namely the recovery time is shorter than the intracavity pulse



duration), the loss factor can be further derived as:

$$\epsilon(\tau, \varphi) = \frac{\epsilon_0}{1 + |\Psi(\tau, \varphi)|^2 \varphi_{SA}/E_{\varphi, SA}} \quad (6)$$

Technically, simulations based on the standard cavity model (Eq. 2) with the loss modulation (Eq. 4) or with the fast SA (Eq. 6) can be directly carried out by means of the split-step Fourier method, while simulations with the slow SA require solving Eq. 5 in each round trip during the circulation of the intracavity field, which is a classic boundary value problem with the forced condition  $\kappa_v(\tau, 0) = \kappa_v(\tau, 2\pi)$ .

### 3. Results and discussion

#### 3.1. Temporal dissipative structures via loss modulation

We first carried out simulations based on the LLE model with transient loss modulation. In the condition  $N = 1$  and  $\epsilon_0 = 20$  (i.e. a strong loss modulation), a stability chart of the intracavity field patterns is illustrated in Fig. 1(b). There are mainly three types of localized field patterns when the pump intensity ( $F^2$ ) is above a threshold for the nonlinear four wave mixing, which are stable solitons, soliton breathers, and chaotic patterns in the operation regime of modulation instability. In particular, it can be observed that the stable soliton state could exist over a wide range of the detuning ( $\Delta$ ) and even exists on the blue-detuned side of the resonance ( $\Delta < 0$ ). Significantly, the soliton peak is located on the minimum of the intracavity loss. Yet, there is a pedestal in the soliton field pattern, which is distinguishable when the system is in the blue-detuned regime, and with an increase of the detuning accessing the red-detuned regime, becomes reduced. In Fig. 1(b), the intensity of the pedestal in the soliton region is reflected on the lightness of the blue shading area.

We showcased a typical set of five consecutive intracavity field patterns from blue detuned side to the red-detuned side, at a constant pump intensity, see Fig. 1(c,d). As a result, the stable soliton state on the blue-detuned side exhibits a narrower comb spectral bandwidth compared with that on the red-detuned side, and both temporal field patterns are characterized to be the Fourier limited pulses with respect to their spectra. In the breathing state, the averaged comb spectrum exhibits a triangle profile, which is similar to previous observations in standard dissipative microresonators [41–45].

We also investigated the stability chart of the intracavity field patterns at different modulation depths of the transient loss factor, see Fig. 2. Together with the chart in Fig. 1(b), an overall evolution of the distribution of the intracavity field patterns is revealed. Given the fact that the overall loss in the system is reduced when the loss modulation depth is decreased, the stability chart is more developed at a high pump intensity side, and overall the intracavity field patterns are enriched. This include the emergence of a second stable soliton region (cf. the red colored region in Fig. 2(a)) and the void region, and the region corresponding to Turing rolls by further decreasing the modulation depth (cf. the brown and the purple regions in Fig. 2(d, g)).

The rich dissipative structures via the loss modulation is determined by a large number of LLE simulations, in which the value of the pump intensity is swept. In each simulation, the soliton state in the red-detuned regime is first probed and evolves to be stabilized, following a backward scan of the detuning to sweep over the resonance [22]. Then, we traced both the peak intensity and the averaged intensity of the intracavity field pattern, which exhibit clear boundaries determining the region of dissipative structures in the system.

Compared with the standard LLE model (where the loss factor is a constant), the presence of the loss modulation leads to an enhancement in the stable dissipative state, which is reflected by the expansion of the stable state region in stability charts.

Of particularly interest is the second stable soliton region that emerges at close-to-zero detuning values, whose temporal field patterns are characterized and compared with the soliton field

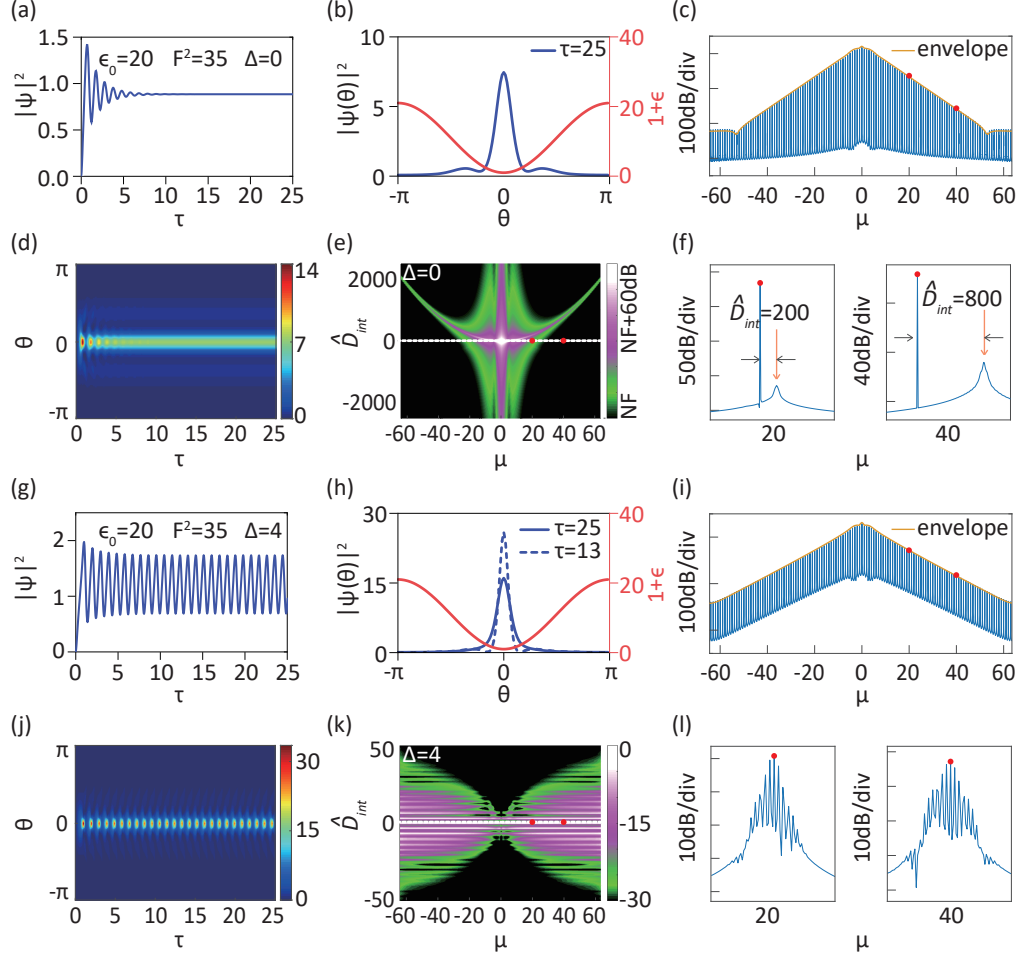


Fig. 3. Self initiated dissipative solitons at close-to-zero detuning. (a, d) Evolution of both the averaged intensity and the intracavity field pattern over cavity round trips, in the system being in resonance (i.e.  $\Delta = 0$ ). (b) The stabilized soliton profile after a few round trips. (c) Simulated soliton comb spectrum in a resolution  $\frac{1}{2^{14}}$  of the repetition frequency. (e) The spectrogram of the soliton frequency comb, at the intensity level around the noise floor, which reveals the distribution of the cavity resonances, equivalently the integrated (normalized) dispersion profile  $\hat{D}_{int} = \frac{1}{2}\mu^2$ . (f) Spectra around selected comb modes with the appearance of close-by resonances. (g-l) A similar investigation but at the detuning  $\Delta = 4$ , where the system is self-evolved to a breathing soliton state. Accordingly in the spectrogram (k), strong modulations is featured around the comb modes, which is also observed in the spectra around selected comb modes (l). Note: the comb spectrum of the soliton breathers was first normalized with respect to the overall envelop, before the spectrogram (k) is generated.

patterns at larger detuning values, see Fig. 2(c, f). Remarkably, this emergent soliton state shows a dual-pulse field pattern, or more specifically evolves from the pedestal of the soliton pattern while the central pulse profile is weakened. As such, this state shares a common feature with the neighbouring void region, both have the central soliton profile suppressed.

### 3.2. Self-starting dissipative solitons

In principle, spontaneous symmetry breaking is the key to trigger the formation of dissipative structures, which can be induced by nonlinear effects in the cavity or via loss fluctuations. The former regime is famous for dissipative microresonator systems where the soliton state exists in the red-detuned regime, while the latter is commonly applied in mode-locked laser systems by means of the saturable absorption. Here, we aimed to combine a dissipative system with loss fluctuations, and investigate dissipative soliton formation operated at zero-detuning (i.e.  $\Delta = 0$ , the system is operated in resonance). As mentioned above, we observed stable soliton states at close-to-zero detuning values. This has paved a way to self-starting dissipative solitons as nonlinear induced bifurcation is not presented in this detuning region and the soliton pattern becomes the only state supported by the system.

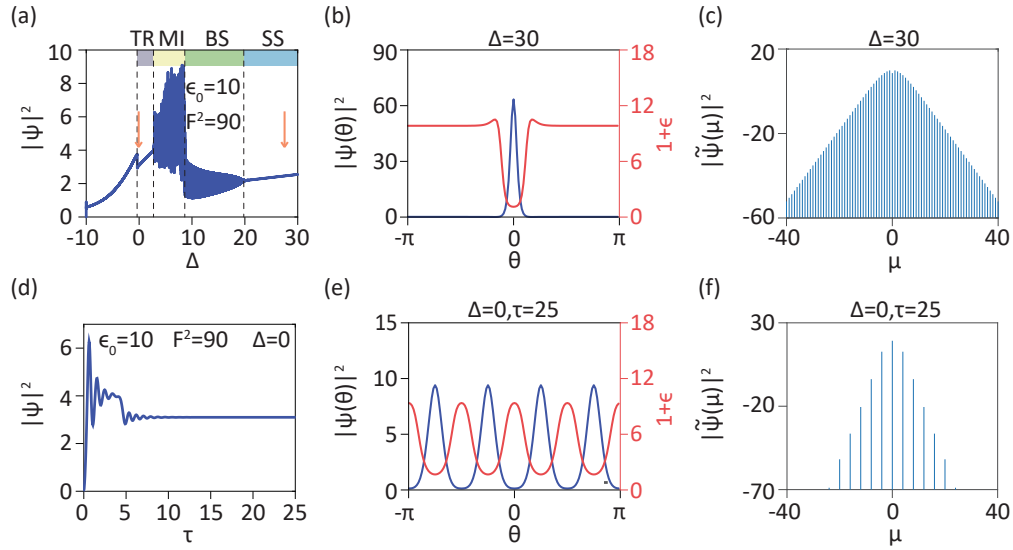


Fig. 4. Dissipative solitons via fast saturable absorption. (a) The averaged intracavity intensity upon the forward scan of the detuning, in the condition that the modulation depth of the saturable absorption is set as  $\epsilon_0 = 10$ . TR: Turing rolls. BS: Breathers. SS: Stable solitons. (b,c) The stabilized temporal soliton pattern along with the intensity-dependent loss profile, and the corresponding comb spectrum, at the detuning  $\Delta = 30$ . (d) Trace of a dissipative structure reached in the system by self-evolution, and being in resonance. (e) The stabilized Turing rolls and the corresponding loss profile upon the self-starting process. (f) The comb spectrum of the Turing rolls. The saturable intensity is  $I_{\varphi,SA} = E_{\varphi,SA}/\varphi_{SA} \approx 0.7$ .

Indeed, we observed the self-starting process for dissipative solitons at close-to-zero detuning values, see Fig. 3. In particular, a stable soliton state is reached at zero-detuning via a strong loss fluctuation ( $\epsilon_0 = 20$ ), see Fig. 3(a,d). The intracavity temporal soliton pattern is presented in Fig. 3(b), in which a small pedestal remains. We simulated a pulse train with  $2^{14}$  solitons and obtained a noise resolved comb spectrum, see Fig. 3(c), in which the cavity cold resonances are resolved and the comb lasing modes are deviated from resonances, see Fig. 3(f). In the spectrogram of the soliton comb, shown in Fig. 3(e), the distribution of the cavity resonances that reflects the profile of the integrated dispersion, is clearly identified. This confirms that the localized field pattern has balanced the dispersive effect in the cavity by the nonlinear effect, and the localized field pattern is a solitary wave. Similarly, the state of the breathing soliton is also reached at a close-to-zero detuning value  $\Delta = 4$ , see Fig. 3(g,h,j). The averaged breather spectrum exhibits a

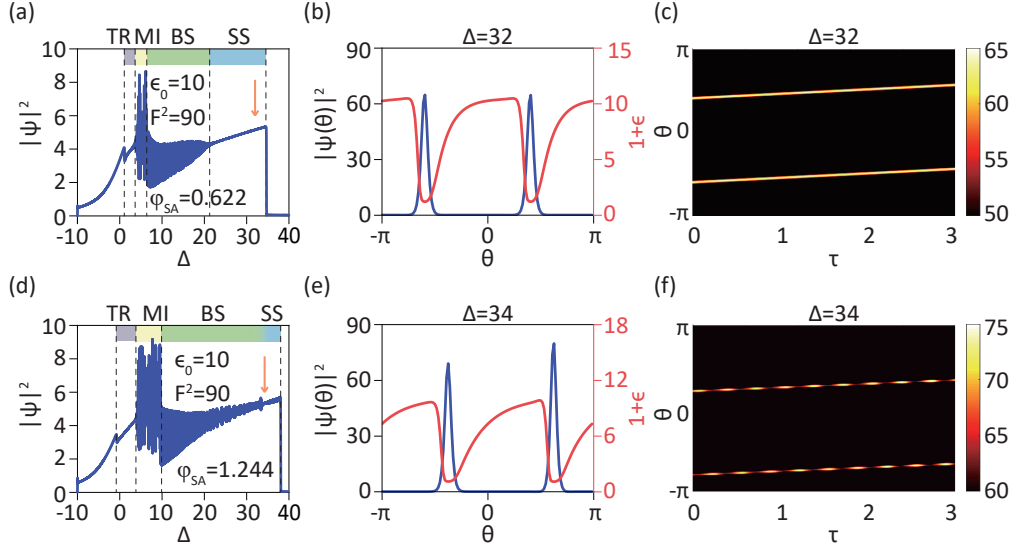


Fig. 5. Dissipative solitons via slow saturable absorption (SA). (a) The averaged intracavity intensity upon the forward scan of the detuning. The modulation depth of the SA is  $\epsilon_0 = 10$ , the recovery time is  $\phi_{SA} \approx 0.6$  and the saturable energy is  $E_{\phi,SA} \approx 0.8$ . TR: Turing rolls. BS: Breathers. SS: Stable solitons. (b) A two soliton pulse state circulating in the cavity, along with the SA-induced loss profile that is asymmetric with respect to the soliton profile. (c) Temporal evolution of the soliton pair over time, when the detuning is fixed at  $\Delta = 32$ . (d, e) Similar to (a, b) in the condition the recovery time is  $\phi_{SA} \approx 1.2$ . (f) Temporal evolution of the soliton pair that features out-of-phase oscillations in the soliton intensity, when the detuning is fixed at  $\Delta = 34$ .

triangle envelop, and strong side-bands are generated around each comb mode, see Fig. 3(i,k,l). As a consequence, the dispersion profile underlying the system is hindered. Therefore, we have demonstrated a self-starting dissipative soliton state operated in resonance.

### 3.3. Stable dissipative structures via saturable absorption

In general, the effect of the saturable absorption (SA) is to introduce an intensity-dependent transmittance to a system and is therefore beneficial to realize pulsed structures [40], which in nature is similar to the effect of the loss modulation. Nevertheless, the difference is that the SA-induced loss fluctuation is simultaneously evolved with the formation of the cavity field pattern. In this way, a positive feedback regime is established in the system, which could initiate the formation of dissipative structures.

To verify this point, we carried out simulations with the SA effect. The results are presented in Fig. 4 and Fig. 5. We first performed the forward laser tuning to investigate possible dissipative structures supported by the system, in the condition of a moderate modulation depth in the SA, i.e.  $\epsilon_0 = 10$ . During the process, Turing rolls, MI state, breathers, and stabilized solitons are observed, see Fig. 4(a). In particular, we noticed that an elongated region for the Turing pattern and a shortened region for the MI state has been supported in the presence of the SA, compared with that by the effect of loss modulation and that in a standard system. This implies that the SA could effectively suppress the chaotic field patterns in the cavity and prefers stabilized dissipative structures. As a transient effect, the fast SA-induced loss profile exhibits a decrease along with the soliton pattern and is symmetric regarding the raising and the ending edges of the soliton pulse profile, Fig. 4(b,c). The self-starting process is also investigated in such a SA-based system

when being operated in resonance, and as a result, Turing rolls are self-initiated and stabilized, see Fig. 4(d,e,f).

Similarly, in the presence of the slow SA effect, both the soliton state and Turing rolls are supported by the system, see Fig. 5(a,d), and Turing rolls can be accessed by self-evolution of the system. In contrast to the fast SA, the slow SA-induced loss profile is asymmetric with respect to the soliton pulse profile, see Fig. 5(b,e). Remarkably, the soliton state (in the form of two soliton pulses circulating in the cavity) are not fully stabilized but featuring slow fluctuation in the intensity, see Fig. 5(c,f). This can be attributed to the relaxation process of the slow SA, namely a long recovery time in the loss profile would interact with the neighbouring soliton pulse in the cavity, leading to a coupled soliton pair featuring energy exchange in between. Indeed, in the condition of a long recovery time in the SA, out-of-phase oscillations in the intensity of the soliton pair are observed, which is the signature of the energy exchange dynamic [46], see Fig. 5(f).

#### 4. Conclusion

In conclusion, we have investigated rich dissipative structures in an optical cavity system with transient loss fluctuation. With a direct modulation on the loss factor, the dissipative system shows a significant change on the supporting states, where stabilized temporal dissipative solitons at close-to-zero detuning values can be supported, and be reached by self-evolution of the system. Moreover, the loss modulation is implemented by the effect of the saturable absorption, with which stabilized patterns close to the Turing rolls can be accessed upon the self-starting process. In practice, introducing the SA effect to Kerr resonators, particularly to optical microresonators, is possible by e.g. coupling with low dimensional active materials such as graphene or quantum dots, while the material induced potential loss can be compensated by the gain regime in the cavity.

Therefore, our work has demonstrated the role of the loss fluctuation in triggering the spontaneous symmetric breaking in dissipative systems and the formation of localized field patterns such as dissipative solitons. Given that active doping of microresonators is a potential trend in the research of soliton micro-combs, such a soliton state may be practically implemented in the near future. Moreover, the self-starting soliton state operated in resonance indicates a high conversion efficiency between the pump wave and the soliton, which is highly desired for applications. Yet, this work is limited to consider only the anomalous dispersion in the cavity. The effect of transient loss fluctuation in normal dispersion cavities requires a further study.

**Funding.** National Natural Science Foundation of China (11974234); National Key Research and Development Program of China (2020YFA0309400); Shanghai Science and Technology Development Foundation (20QA1403500).

**Acknowledgments.** We acknowledge funding from National Natural Science Foundation of China (No. 11974234), Shanghai Science and Technology Development Funds (No. 20QA1403500), and National Key Research and Development Project of China (No. 2020YFA0309400).

**Disclosures.** The authors declare no conflicts of interest.

**Data Availability Statement.** Data and simulation codes related to this work are available through Zoneto at <http://dx.doi.org/xxx>. All other data and findings of this study are available from the corresponding author upon reasonable request.

#### References

1. G. Nicolis and I. Prigogine, "Self-organization in nonequilibrium systems: from dissipative structures to order through fluctuations," Wiley, New York (1977).
2. P. Grelu and N. Akhmediev, "Dissipative solitons for mode-locked lasers," *Nat. Photon.* **6**, 84–92 (2012).
3. P. Del'Haye, A. Schliesser, O. Arcizet, T. Wilken, R. Holzwarth, and T. J. Kippenberg, "Optical frequency comb generation from a monolithic microresonator," *Nature* **450**, 1214–1217 (2007).

4. F. Leo, S. Coen, P. Kockaert, S.-P. Gorza, P. Emplit, and M. Haelterman, "Temporal cavity solitons in one-dimensional Kerr media as bits in an all-optical buffer," *Nat. Photon.* **4**, 471–476 (2010).
5. T. Herr, V. Brasch, J. D. Jost, C. Y. Wang, N. M. Kondratiev, M. L. Gorodetsky, and T. J. Kippenberg, "Temporal solitons in optical microresonators," *Nat. Photon.* **8**, 145–145 (2013).
6. T. J. Kippenberg, A. L. Gaeta, M. Lipson, and M. L. Gorodetsky, "Dissipative Kerr solitons in optical microresonators," *Science* **361**, eaan8083 (2018).
7. P. Marin-Palomo, J. N. Kemal, M. Karpov, A. Kordts, J. Pfeifle, M. H. P. Pfeiffer, P. Trocha, S. Wolf, V. Brasch, M. H. Anderson, R. Rosenberger, K. Vijayan, W. Freude, T. J. Kippenberg, and C. Koos, "Microresonator-based solitons for massively parallel coherent optical communications," *Nature* **546**, 274 (2017).
8. A. Fülöp, M. Mazur, A. Lorences-Riesgo, T. A. Eriksson, P.-H. Wang, Y. Xuan, D. E. Leaird, M. Qi, P. A. Andrekson, A. M. Weiner, and V. Torres-Company, "Long-haul coherent communications using microresonator-based frequency combs," *Opt. Express* **25**, 26678–26688 (2017).
9. A. Fülöp, M. Mazur, A. Lorences-Riesgo, O. B. Helgason, P.-H. Wang, Y. Xuan, D. E. Leaird, M. Qi, P. A. Andrekson, A. M. Weiner, and V. Torres-Company, "High-order coherent communications using mode-locked dark-pulse Kerr combs from microresonators," *Nat. Commun.* **9**, 1598 (2018).
10. B. Corcoran, M. Tan, X. Xu, A. Boes, J. Wu, T. G. Nguyen, S. T. Chu, B. E. Little, R. Morandotti, A. Mitchell, and D. J. Moss, "Ultra-dense optical data transmission over standard fibre with a single chip source," *Nat. Commun.* **11**, 2568 (2020).
11. M.-G. Suh and K. J. Vahala, "Soliton microcomb range measurement," *Science* **359**, 884 (2018).
12. P. Trocha, M. Karpov, D. Ganin, M. H. P. Pfeiffer, A. Kordts, S. Wolf, J. Krockenberger, P. Marin-Palomo, C. Weimann, S. Randel, W. Freude, T. J. Kippenberg, and C. Koos, "Ultrafast optical ranging using microresonator soliton frequency combs," *Science* **359**, 887 (2018).
13. J. Wang, Z. Lu, W. Wang, F. Zhang, J. Chen, Y. Wang, J. Zheng, S. T. Chu, W. Zhao, B. E. Little, X. Qu, and W. Zhang, "Long-distance ranging with high precision using a soliton microcomb," *Photon. Res.* **8**, 1964–1972 (2020).
14. J. Riemensberger, A. Lukashchuk, M. Karpov, W. Weng, E. Lucas, J. Liu, and T. J. Kippenberg, "Massively parallel coherent laser ranging using a soliton microcomb," *Nature* **581**, 164–170 (2020).
15. W. Liang, D. Eliyahu, V. S. Ilchenko, A. A. Savchenkov, A. B. Matsko, D. Seidel, and L. Maleki, "High spectral purity Kerr frequency comb radio frequency photonic oscillator," *Nat. Commun.* **6**, 7957 (2015).
16. J. Liu, E. Lucas, A. S. Raja, J. He, J. Riemensberger, R. N. Wang, M. Karpov, H. Guo, R. Bouchand, and T. J. Kippenberg, "Photonic microwave generation in the X- and K-band using integrated soliton microcombs," *Nat. Photon.* **14**, 486–491 (2020).
17. W. Jin, Q.-F. Yang, L. Chang, B. Shen, H. Wang, M. Leal, L. Wu, M. Gao, A. Feshali, M. Paniccia, K. Vahala, and J. Bowers, "Hertz-linewidth semiconductor lasers using cmos-ready ultra-high-q microresonators," *Nat. Photon.* **15** (2021).
18. E. Obrzud, M. Rainer, A. Harutyunyan, M. H. Anderson, J. Liu, M. Geiselmann, B. Chazelas, S. Kundermann, S. Lecomte, M. Cecconi, A. Ghedina, E. Molinari, F. Pepe, F. Wildi, F. Bouchy, T. J. Kippenberg, and T. Herr, "A microphotonic astrocomb," *Nat. Photon.* **13**, 31–35 (2019).
19. M.-G. Suh, X. Yi, Y.-H. Lai, S. Leifer, I. S. Grudinin, G. Vasisht, E. C. Martin, M. P. Fitzgerald, G. Doppmann, J. Wang, D. Mawet, S. B. Papp, S. A. Diddams, C. Beichman, and K. Vahala, "Searching for exoplanets using a microresonator astrocomb," *Nat. Photon.* **13**, 25–30 (2019).
20. J. Feldmann, N. Youngblood, M. Karpov, H. Gehring, X. Li, M. Stappers, M. Le Gallo, X. Fu, A. Lukashchuk, A. S. Raja, J. Liu, C. D. Wright, A. Sebastian, T. J. Kippenberg, W. H. P. Pernice, and H. Bhaskaran, "Parallel convolutional processing using an integrated photonic tensor core," *Nature* **589**, 52–58 (2021).
21. X. Xu, M. Tan, B. Corcoran, J. Wu, A. Boes, T. G. Nguyen, S. T. Chu, B. E. Little, D. G. Hicks, R. Morandotti, A. Mitchell, and D. J. Moss, "11 TOPS photonic convolutional accelerator for optical neural networks," *Nature* **589**, 44–51 (2021).
22. H. Guo, M. Karpov, E. Lucas, A. Kordts, M. Pfeiffer, V. Brasch, G. Lihachev, V. Lobanov, M. Gorodetsky, and T. Kippenberg, "Universal dynamics and deterministic switching of dissipative Kerr solitons in optical microresonators," *Nat. Phys.* **13**, 94 (2016).
23. J. R. Stone, T. C. Briles, T. E. Drake, D. T. Spencer, D. R. Carlson, S. A. Diddams, and S. B. Papp, "Thermal and nonlinear dissipative-soliton dynamics in Kerr-microresonator frequency combs," *Phys. Rev. Lett.* **121**, 063902 (2018).
24. C. Joshi, J. K. Jang, K. Luke, X. Ji, S. A. Miller, A. Klenner, Y. Okawachi, M. Lipson, and A. L. Gaeta, "Thermally controlled comb generation and soliton modelocking in microresonators," *Opt. Lett.* **41**, 2565–2568 (2016).
25. J. Liu, H. Tian, E. Lucas, A. S. Raja, G. Lihachev, R. N. Wang, J. He, T. Liu, M. H. Anderson, W. Weng, S. A. Bhawe, and T. J. Kippenberg, "Monolithic piezoelectric control of soliton microcombs," *Nature* **583**, 385–390 (2020).
26. D. C. Cole, J. R. Stone, M. Erkintalo, K. Y. Yang, X. Yi, K. J. Vahala, and S. B. Papp, "Kerr-microresonator solitons from a chirped background," *Optica* **5**, 1304–1310 (2018).
27. H. Zhou, Y. Geng, W. Cui, S.-W. Huang, Q. Zhou, K. Qiu, and C. Wei Wong, "Soliton bursts and deterministic dissipative Kerr soliton generation in auxiliary-assisted microcavities," *Light. Sci. Appl.* **8**, 50 (2019).
28. N. G. Pavlov, S. Koptyaev, G. V. Lihachev, A. S. Voloshin, A. S. Gorodnitskiy, M. V. Ryabko, S. V. Polonsky, and M. L. Gorodetsky, "Narrow-linewidth lasing and soliton Kerr microcombs with ordinary laser diodes," *Nat. Photon.*

- 12, 694–698 (2018).
29. B. Stern, X. Ji, Y. Okawachi, A. L. Gaeta, and M. Lipson, “Battery-operated integrated frequency comb generator,” *Nature* **562**, 401–405 (2018).
30. A. S. Raja, A. S. Voloshin, H. Guo, S. E. Agafonova, J. Liu, A. S. Gorodnitskiy, M. Karpov, N. G. Pavlov, E. Lucas, R. R. Galiev, A. E. Shitikov, J. D. Jost, M. L. Gorodetsky, and T. J. Kippenberg, “Electrically pumped photonic integrated soliton microcomb,” *Nat. Commun.* **10**, 680 (2019).
31. B. Shen, L. Chang, J. Liu, H. Wang, Q.-F. Yang, C. Xiang, R. N. Wang, J. He, T. Liu, W. Xie, J. Guo, D. Kinghorn, L. Wu, Q.-X. Ji, T. J. Kippenberg, K. Vahala, and J. E. Bowers, “Integrated turnkey soliton microcombs,” *Nature* **582**, 365–369 (2020).
32. A. S. Voloshin, N. M. Kondratiev, G. V. Lihachev, J. Liu, V. E. Lobanov, N. Y. Dmitriev, W. Weng, T. J. Kippenberg, and I. A. Bilenko, “Dynamics of soliton self-injection locking in optical microresonators,” *Nat. Commun.* **12**, 235 (2021).
33. T. C. Briles, S.-P. Yu, L. Chang, C. Xiang, J. Guo, D. Kinghorn, G. Moille, K. Srinivasan, J. E. Bowers, and S. B. Papp, “Hybrid InP and SiN integration of an octave-spanning frequency comb,” *APL Photonics* **6**, 026102 (2021).
34. C. Xiang, J. Liu, J. Guo, L. Chang, R. N. Wang, W. Weng, J. Peters, W. Xie, Z. Zhang, J. Riemensberger, J. Selvidge, T. J. Kippenberg, and J. E. Bowers, “Laser soliton microcombs on silicon,” *arXiv:2103.02725 arXiv:2103.02725* (2021).
35. B. Yao, S.-W. Huang, Y. Liu, A. K. Vinod, C. Choi, M. Hoff, Y. Li, M. Yu, Z. Feng, D.-L. Kwong, Y. Huang, Y. Rao, X. Duan, and C. W. Wong, “Gate-tunable frequency combs in graphene–nitride microresonators,” *Nature* **558**, 410–414 (2018).
36. Q. Bao, H. Zhang, Y. Wang, Z. Ni, Y. Yan, Z. X. Shen, K. P. Loh, and D. Y. Tang, “Atomic-layer graphene as a saturable absorber for ultrafast pulsed lasers,” *Adv. Mater.* **19**, 3077–3083 (2009).
37. Z. Sun, T. Hasan, F. Torrisi, D. Popa, G. Privitera, F. Wang, F. Bonaccorso, D. M. Basko, and A. C. Ferrari, “Graphene mode-locked ultrafast laser,” *ACS Nano* **4**, 803–810 (2010).
38. C. Qin, K. Jia, Q. Li, T. Tan, X. Wang, Y. Guo, S.-W. Huang, Y. Liu, S. Zhu, Z. Xie, Y. Rao, and B. Yao, “Electrically controllable laser frequency combs in graphene-fibre microresonators,” *Light. Sci. Appl.* **9**, 185 (2020).
39. L. A. Lugiato and R. Lefever, “Spatial dissipative structures in passive optical systems,” *Phys. Rev. Lett.* **58**, 2209–2211 (1987).
40. F. X. Kurtner, J. A. der Au, and U. Keller, “Mode-locking with slow and fast saturable absorbers-what’s the difference?” *IEEE J. Sel. Top. Quantum Electron.* **4**, 159–168 (1998).
41. F. Leo, L. Gelens, P. Emplit, M. Haelterman, and S. Coen, “Dynamics of one-dimensional Kerr cavity solitons,” *Opt. Express* **21**, 9180–9191 (2013).
42. C. Bao, J. A. Jaramillo-Villegas, Y. Xuan, D. E. Leaird, M. Qi, and A. M. Weiner, “Observation of Fermi-Pasta-Ulam Recurrence Induced by Breather Solitons in an Optical Microresonator,” *Phys. Rev. Lett.* **117**, 163901 (2016).
43. M. Yu, J. K. Jang, Y. Okawachi, A. G. Griffith, K. Luke, S. A. Miller, X. Ji, M. Lipson, and A. L. Gaeta, “Breather soliton dynamics in microresonators,” *Nat. Commun.* **8**, 14569 (2017).
44. E. Lucas, M. Karpov, H. Guo, M. L. Gorodetsky, and T. J. Kippenberg, “Breathing dissipative solitons in optical microresonators,” *Nat. Commun.* **8**, 736 (2017).
45. S. Wan, R. Niu, Z.-Y. Wang, J.-L. Peng, M. Li, J. Li, G.-C. Guo, C.-L. Zou, and C.-H. Dong, “Frequency stabilization and tuning of breathing solitons in si<sub>3</sub>n<sub>4</sub> microresonators,” *Photon. Res.* **8**, 1342–1349 (2020).
46. H. Guo, E. Lucas, M. H. Pfeiffer, M. Karpov, M. Anderson, J. Liu, M. Geiselmann, J. D. Jost, and T. J. Kippenberg, “Intermode breather solitons in optical microresonators,” *Phys. Rev. X* **7**, 041055 (2017).